

Electronic Supplementary Information

Design of TPGS-functionalized Cu_3BiS_3 nanocrystals with strong absorption in the second near-infrared window for radiation therapy enhancement

Jiangfeng Du,^{a,b,†} Xiaopeng Zheng,^{b,†} Yuan Yong,^b Jie Yu,^b Xinghua Dong,^{b,d} Chenyang Zhang,^b Ruyi Zhou,^b Bai Li,^b Liang Yan,^{*b,d} Chunying Chen,^{*c} Zhanjun Gu,^{*b,d} Yuliang Zhao^{b,c,d}

^a School for Radiological and Interdisciplinary Sciences (RAD-X), Collaborative Innovation Center of Radiation Medicine of Jiangsu Higher Education Institutions, Soochow University, Suzhou 215123, P. R. China

^b CAS Key Laboratory for Biomedical Effects of Nanomaterials and Nanosafety, Institute of High Energy Physics, Chinese Academy of Sciences, Beijing 100049, China

^c CAS Key Laboratory for Biomedical Effects of Nanomaterials and Nanosafety & CAS Center for Excellence in Nanosciences, National Center for Nanoscience and Technology of China, Beijing 100190, P.R. China

^d University of Chinese Academy of Sciences, Beijing 101408, China

E-mail: yanliang@ihep.ac.cn; chenchy@nanoctr.cn; zjgu@ihep.ac.cn

† These authors contributed equally.

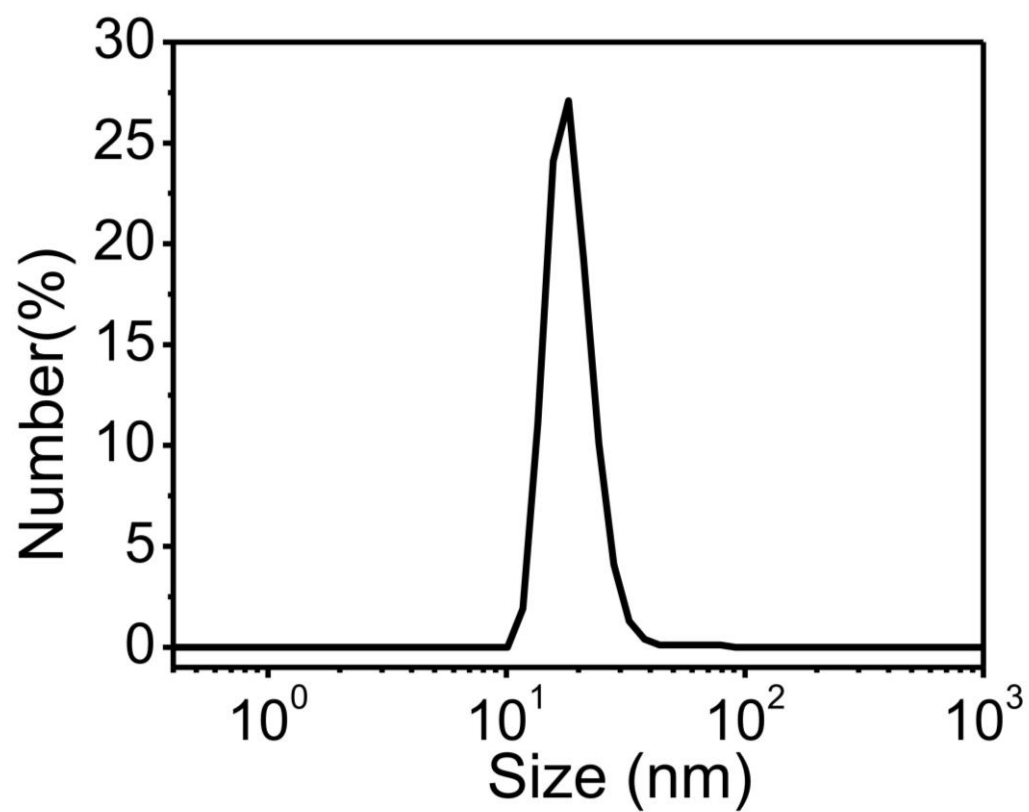


Fig. S1 Hydrodynamic diameter of TPGS-Cu₃BiS₃ in aqueous dispersion.

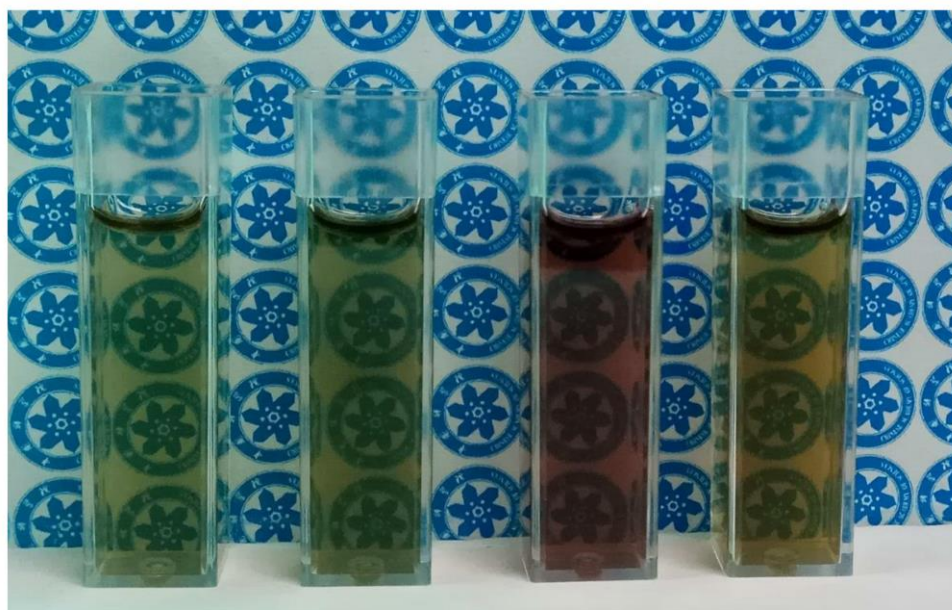


Fig. S2 Photograph of TPGS-Cu₃BiS₃ NCs in different solutions including deionized water, PBS, RPMI-1640, and FBS, from left to right.

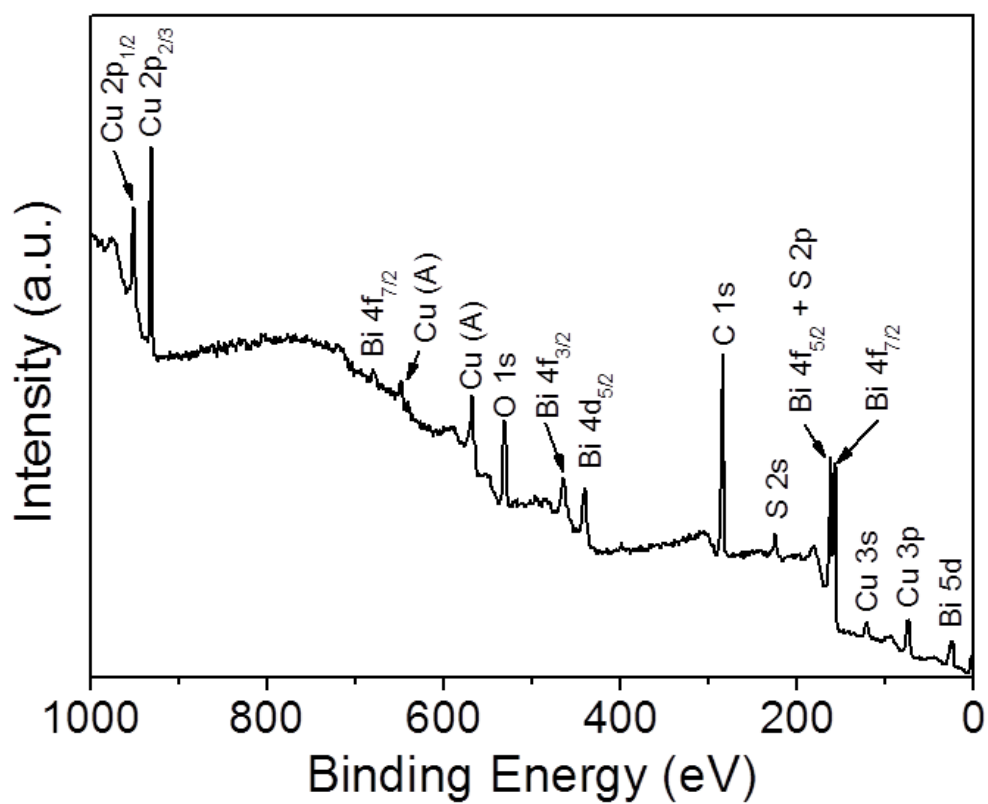


Fig. S3 Wide-scan XPS spectrum of TPGS-Cu₃BiS₃ NCs.

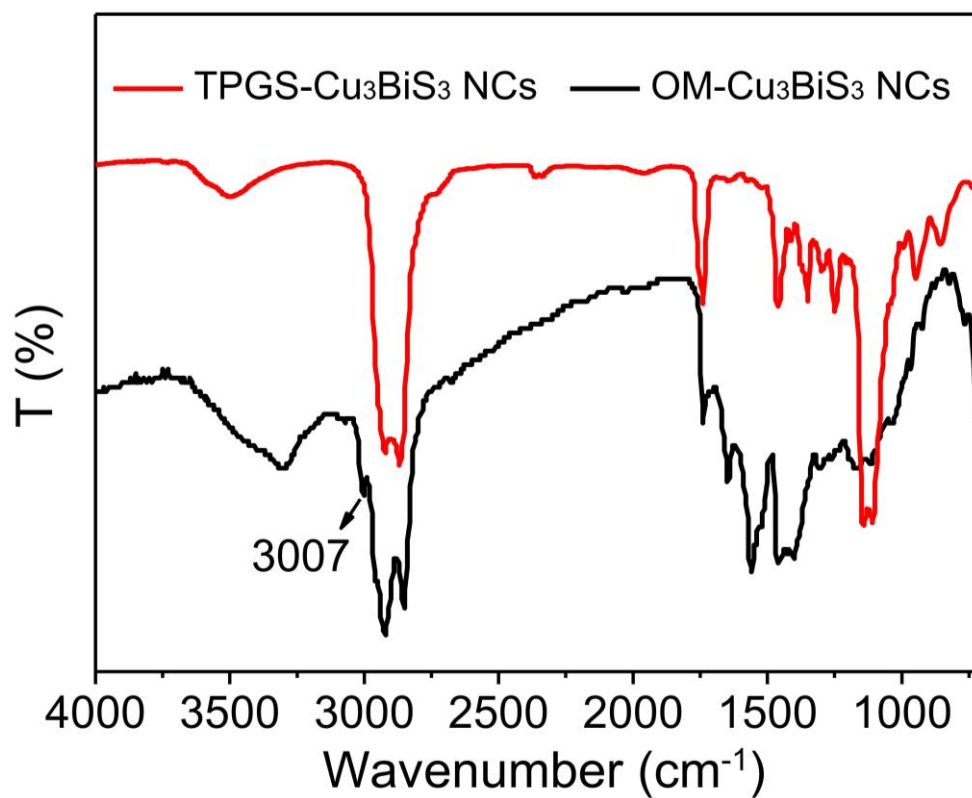


Fig. S4 FT-IR spectra of OM-Cu₃BiS₃ NCs and TPGS-Cu₃BiS₃ NCs.

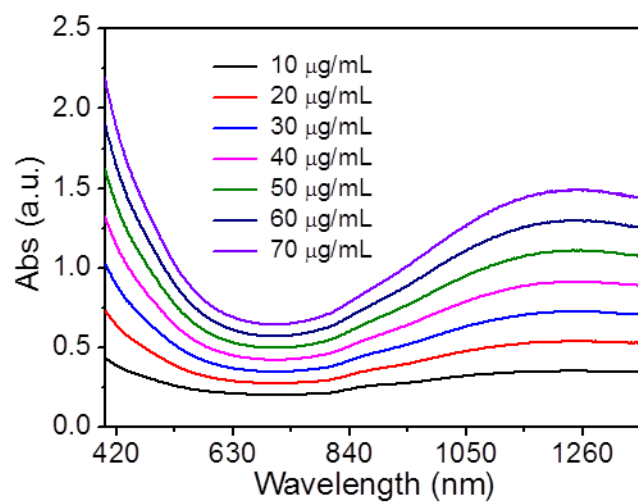


Fig. S5 UV-Vis-NIR absorbance spectra of TPGS-Cu₃BiS₃ NCs in aqueous dispersions with various concentrations.

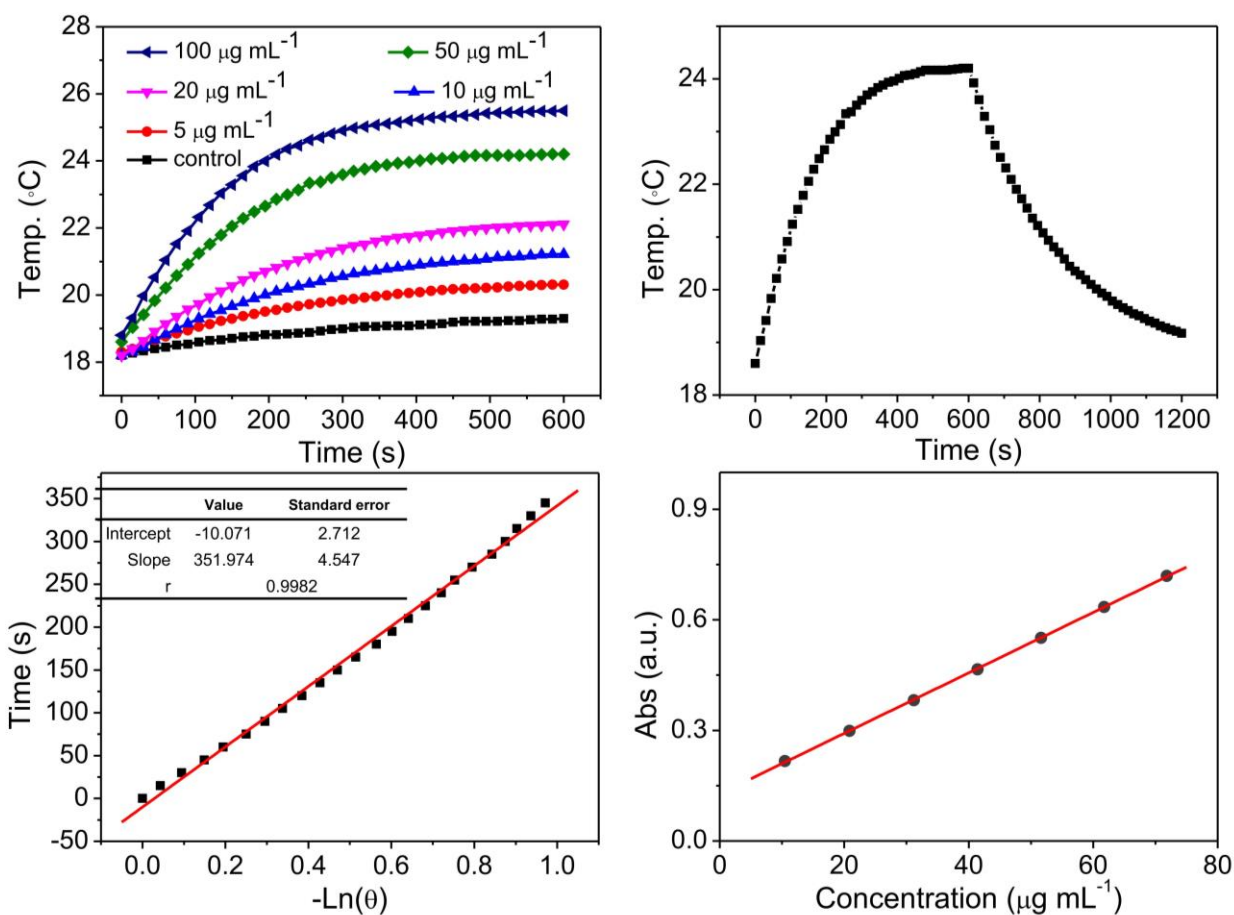


Fig. S6 (a) Temperature elevation curves of aqueous dispersion of TPGS-Cu₃BiS₃ NCs at different concentrations under 808 nm laser irradiation (0.5 W cm^{-2}). (b) Photothermal effect of the irradiation lasted for 10 min, and then the laser was turned off. (c) Plot of cooling time versus negative natural logarithm of the temperature driving force temperature ($-\ln\theta$) which is obtained from the cooling stage. (d) Absorbance versus different concentrations of TPGS-Cu₃BiS₃ NCs at 808 nm wavelength.

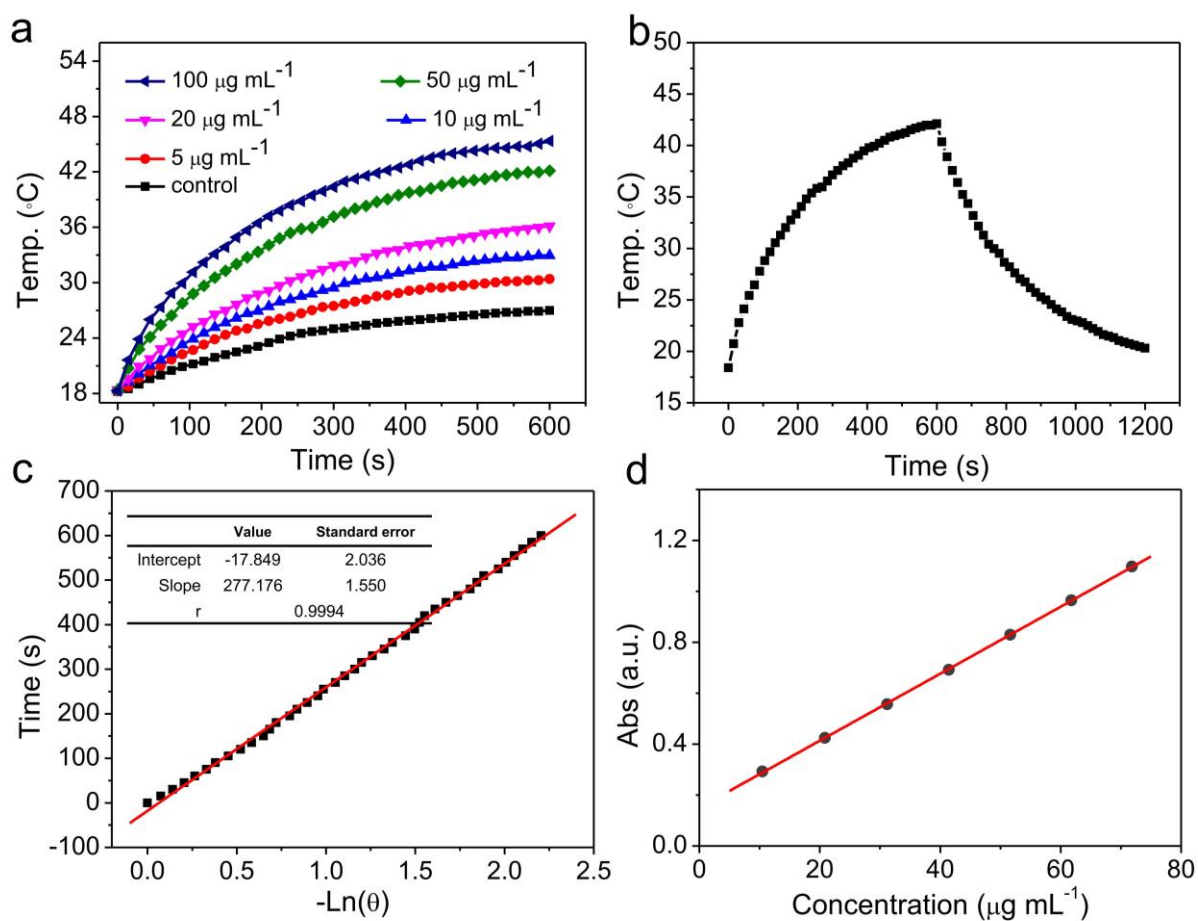


Fig. S7 (a) Temperature elevation curves of aqueous dispersion of TPGS-Cu₃BiS₃ NCs at different concentrations under 980 nm laser irradiation (0.5 W cm⁻²). (b) Photothermal effect of the irradiation lasted for 10 min, and then the laser was turned off. (c) Plot of cooling time versus negative natural logarithm of the temperature driving force temperature ($-\ln(\theta)$) which is obtained from the cooling stage. (d) Absorbance versus different concentrations of TPGS-Cu₃BiS₃ NCs at 980 nm wavelength.

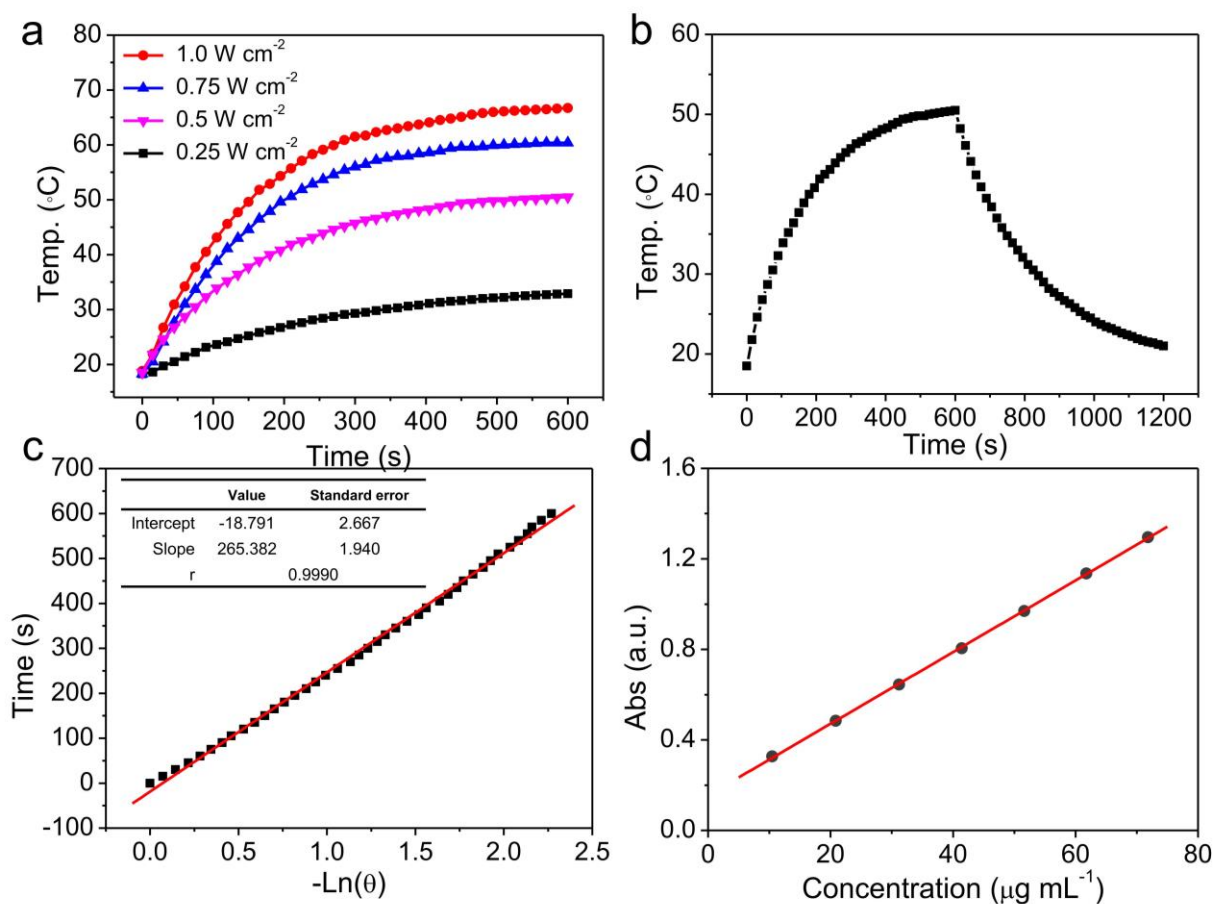


Fig. S8 (a) Temperature elevation curves of aqueous dispersion of TPGS-Cu₃BiS₃ NCs at different power density under 1064 nm laser irradiation. (b) Photothermal effect of the irradiation lasted for 10 min, and then the laser was turned off. (c) Plot of cooling time versus negative natural logarithm of the temperature driving force temperature (-lnθ) which is obtained from the cooling stage. (d) Absorbance versus different concentrations of TPGS-Cu₃BiS₃ NCs at 1064 nm wavelength.

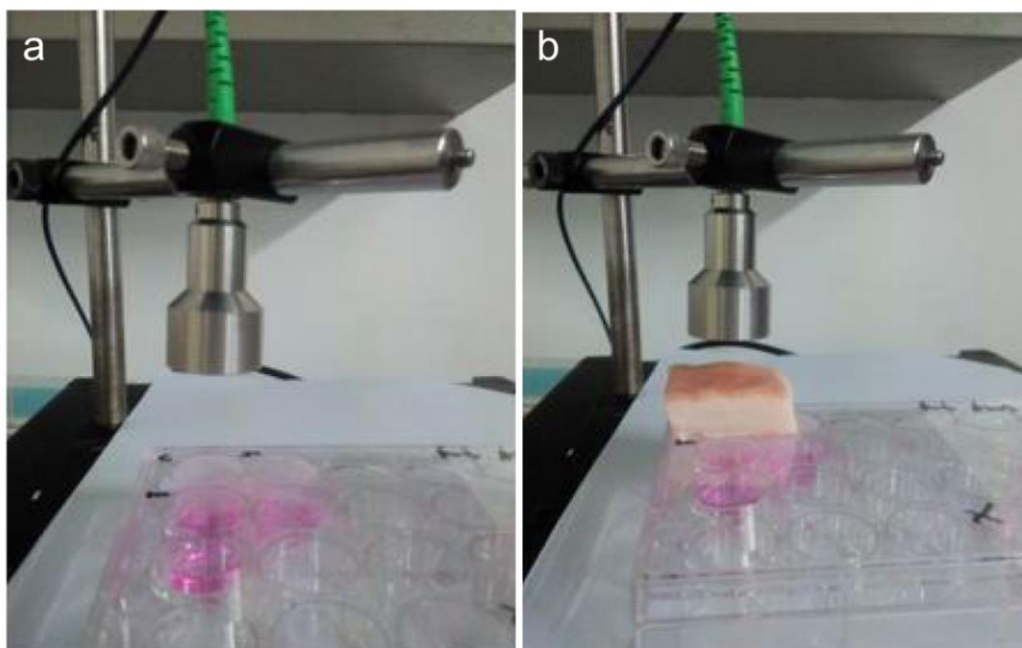


Fig. S9 Photographs of the aqueous dispersion of TPGS-Cu₃BiS₃ NCs under different laser irradiation without (a) or with (b) pork as a laser blocker over a period of 600 s. (0.5 W cm^{-2})

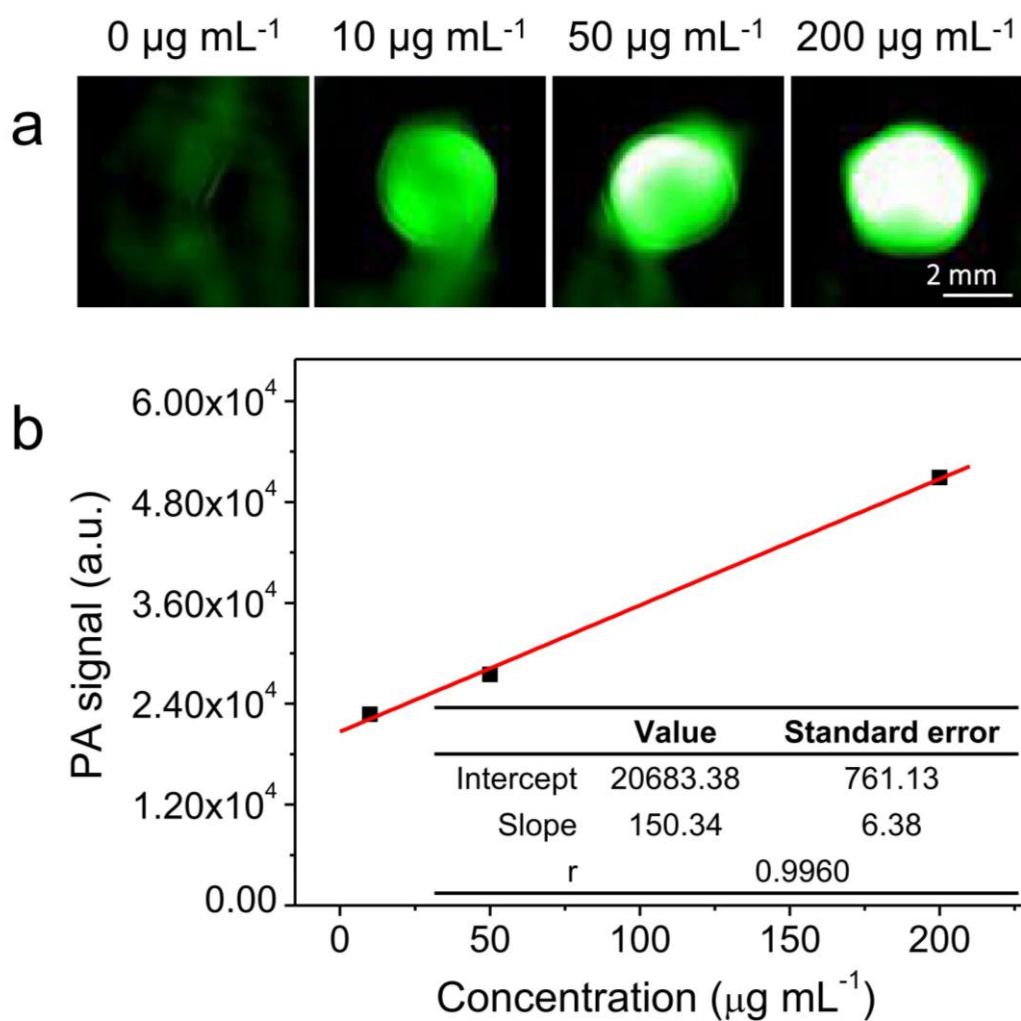


Fig. S10 (a) PA phantom images of the aqueous dispersion of TPGS-Cu₃BiS₃ NCs with different concentrations in the first NIR window. (b) Plots of PA signal versus different concentrations of TPGS-Cu₃BiS₃ NCs. (the laser light range: 900-1200 nm for in vitro imaging)

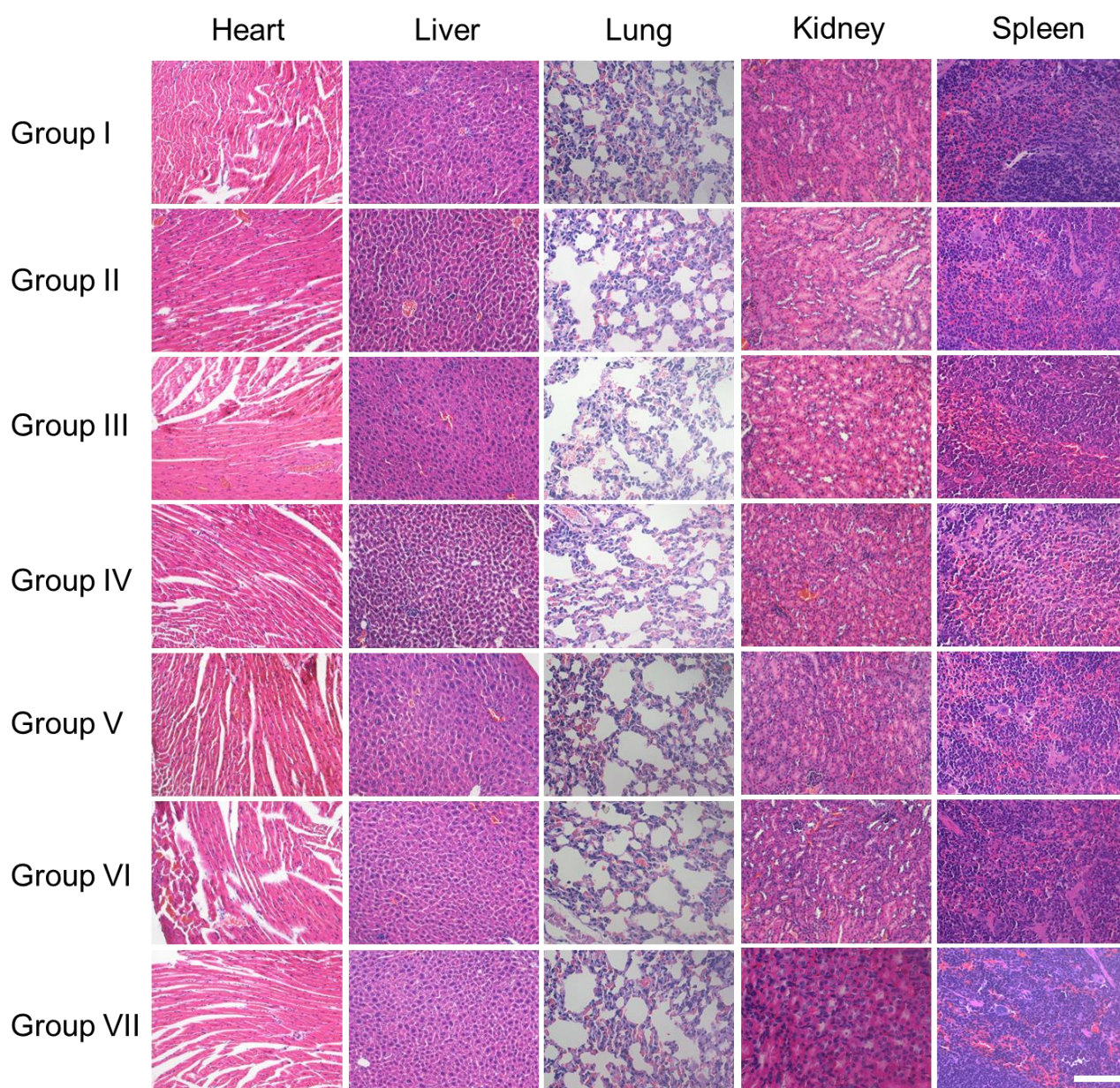


Fig. S11 H&E stained tissue sections from the mice to monitor the histological changes in heart, liver, lung, kidney, spleen and tumor of mice after administrator for 22 days. The scale bar represents 200 μm .

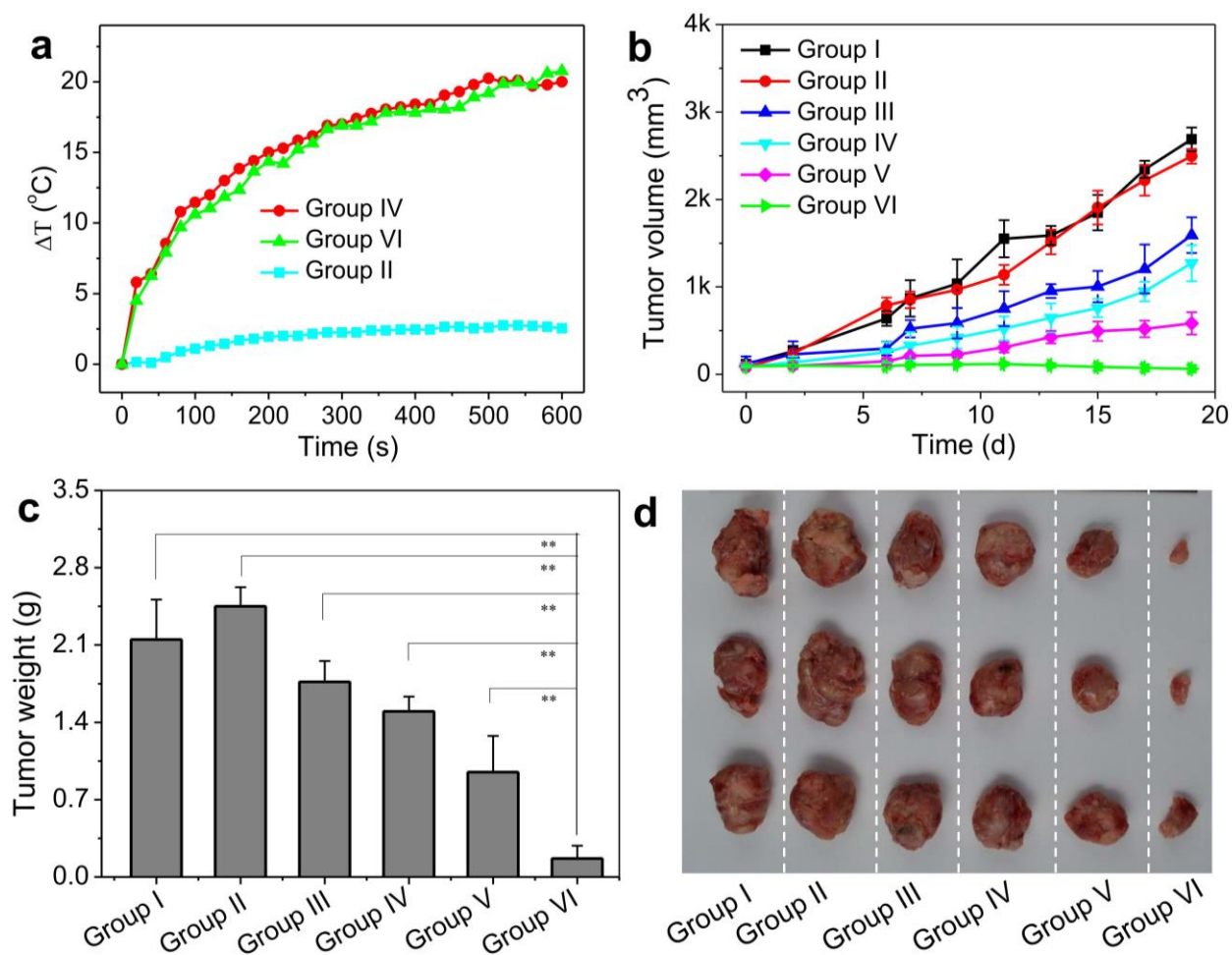


Fig. S12 (a) Temperature changes of tumors monitored by the IR thermal camera during 808 nm laser irradiation. (b) Tumor volume growth curves of different groups of mice after various treatments Groups (n=3). (c) Average weights of tumors collected from the mice at the end of photothermal therapy. * $p < 0.1$, ** $p < 0.01$. (d) Photos of tumors collected from different groups of mice at the end of treatment. Group I: control; Group II: laser; Group III: RT (i); Group IV: PTT(i); Group V: NCs + RT; Group VI: NCs + RT + PTT(i). (1 W cm^{-2} and 10 min)

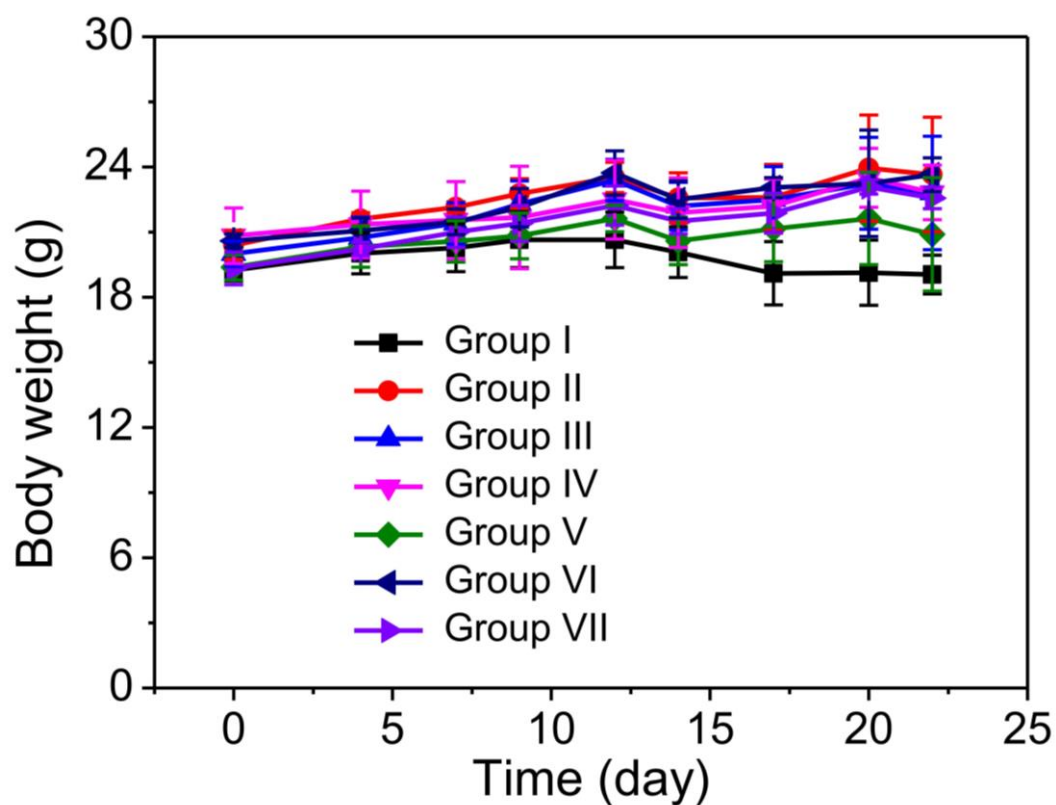


Fig. S13 The weight of Bel-7402 tumor-bearing mice in our observation period in 1064 nm laser treatment.

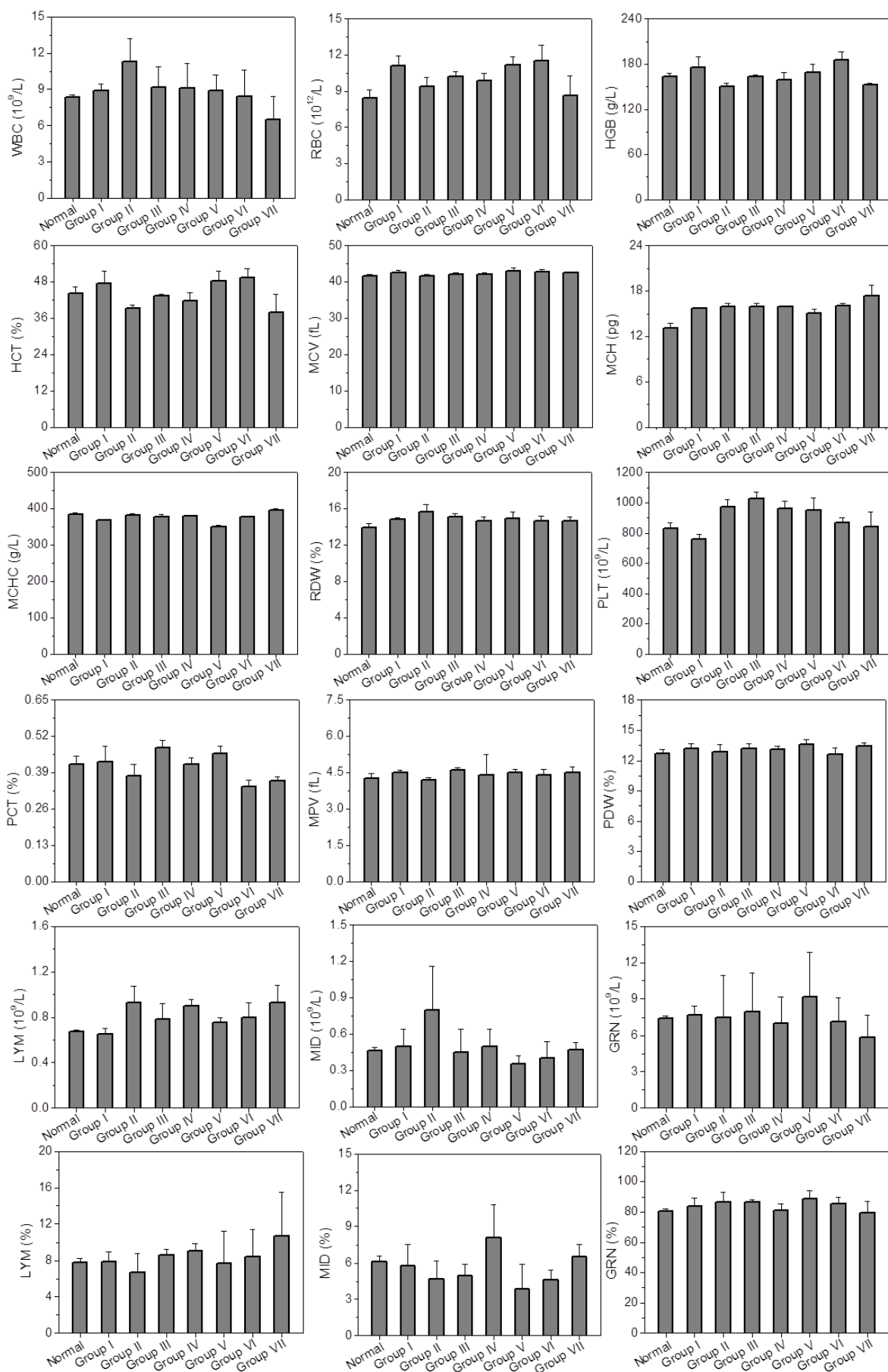


Fig. S14 Blood routine analysis of mice treated with different manner.